Dynamic Behavior of a Porous Char Particle Burning in an Oxygen-Containing Environment

Part I: Constant Particle Radius

S. V. SOTIRCHOS and
N. R. AMUNDSON

University of Houston
Houston, TX 77004

The transient combustion of porous char particles is modelled. The model takes into account the reactions of carbon with CO_2 and O_2 and the oxidation of CO in the gas phase. It reveals strong effects of the intraparticle thermal gradients and of the pore structure evolution scheme on the burning time and predicts an optimum particle size that gives minimum burning time.

SCOPE

Formulating mathematical models describing the behavior of a combustion or gasification reactor or even of a cloud of coal dust, we usually include in the analysis submodels simulating the transient combustion or gasification of the individual microsystems, char or coal particles. It is understandable that these submodels must be simple and, if possible, analytically or semianalytically tractable. Unfortunately, the dynamic behavior of the individual subsystems is very complex, a result of the strong interplay between diffusion and reaction. In particular, the combustion of a porous char particle involves not only diffusion of oxygen and carbon dioxide through the surrounding gas phase and the pores of char and reaction of these two species with carbon, but also oxidation of carbon monoxide produced by the heterogeneous reactions in the gas phase. Moreover, because of local depletion of the solid material, the pore structure of the solid changes spatially and temporally, its evolution involving pore growth, coalescence of adjacent pores, as well as initiation of new pores. Therefore, the study of the combustion of a single char particle with the goal of understanding the effect of every assumption and simplification on the solution structure and identifying suitable simple models reproducing to a satisfactory degree most of the quantitative and qualitative features of the solution does not appear to be an easy task.

This study aims to investigate the dynamic behavior of porous char particles exposed to an oxidizing environment. As the pseudosteady-state analysis of the problem has shown (Sotirchos and Amundson, 1984b), consideration of intraparticle thermal gradients in the mathematical model has strong quantitative and qualitative effects on the pseudosteady-state behavior of the system. In addition, the solution structure has been found to be very sensitive to the reactivity of the char sample. Since this varies with the pore structure characteristics, different modes of pore structure evolution may lead to significant differences in the predicted burning times. Thus, although the model is fairly general describing the diffusion and reaction process both in the interior of the particle and in the surrounding gas phase, we chiefly focus on the effects of intraparticle thermal gradients and of the evolving pore structure on the transient behavior of the reacting particles. According to the assumptions on which the model is built, the properties of the porous matrix evolve spatially and temporally, but locally they are completely determined by the conversion. In other words, the properties of the solid at any conversion level are given by those functions of conversion that describe the evolution of the pore structure of the solid in the kinetically-controlled regime.

CONCLUSIONS AND SIGNIFICANCE

A transient model has been developed describing the dynamic behavior of char particles exposed to an oxygen-containing environment. The model has been used mainly to study the effects of intraparticle thermal gradients and of the evolving char pore structure on the ignition and extinction characteristics of porous char particles of constant radius. According to the model assumptions, the evolution of the char pore structure is determined mostly by the functional dependence of the specific internal surface area on the conversion, which is implicitly given by the dependence of the heterogeneous reaction rates per unit volume on the conversion at constant reactant concentration and constant temperature. Two qualitatively different pore evolution schemes have been considered; a scheme in which the heterogeneous reaction rates per unit of particle volume decrease monotonically with the conversion (pattern *P*1), and another where they go through a maximum (*P*2).

The results have revealed strong effects of intraparticle thermal gradients on the ignition and extinction phenomena observed, and hence on the predicted burning times. Isothermal particles of low initial temperature ignite at considerably higher ambient temperature than the respective nonisothermal particles, and when they do so, they subsequently suffer extinction at a much lower average conversion. As a result, the burning times of isothermal particles are always higher, and the burning structure of the system presents a large transition regime between the regions of complete kinetic and complete diffusion control. In the last two regions, both versions of the model, isothermal and nonisothermal, give similar results, but in the transition regime the difference of their predictions are in some cases larger than one order of magnitude.

As expected, different modes of pore structure evolution predict different burning times in the kinetically-controlled regime, but they also influence strongly the solution structure in the transition regime, both qualitatively and quantitatively. Particles with low initial temperature and pore structure

Current address of S. V. Sotirchos: Dept. of Chemical Engineering, University of Rochester, Rochester, NY 14627.

evolving according to pattern *P*1 ignite only when they enter the ignition regime of the initial pseudosteady-state structure, where only an ignited steady state is possible. A particle reacting according to scheme *P*2, however, may ignite at lower ambient temperatures after spending a considerable part of its lifetime in an unignited state. This phenomenon leads to very large differences in the predicted burning times in the transition regime. The differences are larger between nonisothermal *P*1 and *P*2 particles, but the region of temperature in which they exist is narrower.

There is a critical ambient temperature above which a particle of low initial temperature can ignite. Similarly, at a given ambient temperature, particles of low temperature cannot ignite unless their size is higher than a critical value. Close to the critical size for ignition, the model predicts an optimum value of particle radius that gives minimum burning time. This result is in qualitative agreement with the experimental evidence (Ross and Davidson, 1982) that theoretically predicted burning times of small particles for diffusionally-controlled behavior may be much smaller than the experimentally observed value.

In general, our results have shown that there is a wide range of ambient temperature and particle radius in which knowledge of both the kinetics and intraparticle diffusion characteristics is necessary for the study of the behavior of burning char particles. This region, along with the kinetically-controlled regime, covers a meaningful range of the operational conditions used in practice, especially for small particle sizes (pulverized fuel). Since the pore structure characteristics of the burning particles change continuously with time, even particles that start reacting in the diffusionally-controlled regime may eventually spend a great part of their lifetime in the transition regime and in the kinetically-controlled regime. Consequently, a more accurate characterization of the internal pore structure of the solid and of the way in which it evolves with time is necessary for modelling work.

A large number of theoretical studies dealing with the combustion problem of single particles have appeared. Most of these studies fall into two general categories of models: 1. models of the boundary layer diffusion and reaction problem, the so-called shrinking core models; and 2. models of the intraparticle problem only. The shrinking core models usually lump, sometimes arbitrarily, all the intraparticle diffusion and reaction details on the external surface of the particle and assume that only the radius of the particle or of the unreacted core changes with the conversion. Obviously, the boundary layer diffusion and reaction models are inherently inadequate for investigating the dynamic behavior of a *porous char particle* unless the particle is practically impervious to diffusion or all heterogeneous reactions are controlled by diffusion in the surrounding gas phase. The lumped kinetics, based on the external surface area, strongly depend on the intraparticle diffusion and reaction characteristics which change continuously as the reaction proceeds; on the other hand, in the kinetically controlled regime and in the lower part of the transition regime, the only parameter of the porous particle that practically does not change with the extent of the combustion, up to certain conversion level, is its radius (Dutta et al., 1977). Nevertheless, the shrinking core models (Mon and Amundson, 1980; Sundaresan and Amundson, 1981) revealed some interesting phenomena associated with the combustion of char particles, like critical initial temperatures for ignition and extinction after some conversion level. Also, their results regarding the effect of the ambient conditions on the above phenomena were found to be in qualitative agreement with the experimental evidence (Ubhayakar and Williams, 1976).

Most of the intraparticle models, on the other hand, basically deal with the pore structure evolution problem in the kinetically-controlled regime (e.g., Hashimoto and Silveston, 1973a; Bhatia and Perlmutter, 1979; Simons and Finson, 1979; Gavalas, 1980; Zygourakis et al., 1982). They usually refer to the gasification of char by CO_2, but in the kinetically-controlled regime it is immaterial which is the reactive species as the pore structure properties are solely determined by the conversion. Extensions of these works in the transition and diffusionally-controlled regimes of gasification, where the temperature differences still have minor effects on the solution, have also been presented (Hashimoto and Silveston, 1973b; Simons, 1979; Bhatia and Perlmutter, 1981). Also, Gavalas (1981) extended his work to describe the combustion of char particles, but he treated the particle temperature as a model parameter.

A model for the transient combustion of porous carbon spheres including diffusion and reaction in the surrounding gas phase was developed by Kurylko and Essenhigh (1973). The model was used to explain the experimentally-observed oscillatory combustion of porous spheres of carbon, but no results regarding the structure of the solution or the effect of the several parameters on the burning time were presented. The intraparticle combustion problem was more fully studied by Srinivas and Amundson (1981) using a simplified model (independent diffusion and no intraparticle thermal gradients). As regards the extinction and ignition characteristics of the process, their results led to conclusions qualitatively similar to the predictions of the shrinking core models. Their model is close to the actual problem, but it still leaves out the homogeneous reaction which may cause a substantial part of the pathology of the system. Also, the intraparticle thermal gradients may become important at higher conversions, especially if, as it was assumed, the ash left after depletion of the combustible solid retains its structure.

In this study, we will investigate the behavior of the general system taking into account both the intraparticle problem and the diffusion and reaction phenomena in the surrounding gas phase. One of the main assumptions involved in the development of the mathematical model is that the radius of the particle does not change during the process. We must point out, however, that if the ash layer peels off or if the particle shrinks in one way or another, its dynamic behavior may be significantly different owing to the strong effect of particle size on the pseudosteady-state structure of the problem (Sotirchos and Amundson, 1984b). Transient results for a striking particle will be presented in the second part of this study.

DEVELOPMENT OF THE MODEL

Char Pore Structure

Several experimental studies (Laurendeau, 1978) suggest that coal and char are characterized by a strongly bimodal pore-size distribution. The macropores, which are usually the main transport arteries of the porous solid, account for most of the porosity, while the small pores, lying in the mesopore and in the micropore range, account for nearly all the available surface area. Such a pore-size distribution will be considered here. The same pore structure was espoused in our previous papers (Sotirchos and Amundson, 1984a,b) where we introduced some additional assumptions. That is, we considered that the macropores form a highly interconnected network of pores from which short small pores emanate and that locally we have complete utilization of the internal surface area of each small pore. The last assumption resulted from some calculations (Sotirchos and Amundson, 1984a) that showed that the effectiveness factor of the individual small pores takes values close to unity at temperatures less than 1,600 K, even for large length to diameter ratios. Eventually, as the simulation results will show, the model appears to be valid in the whole temperature range considered since at temperatures higher than 1,600 K the combustion process is controlled by diffusion in the boundary layer;

consequently, the intraparticle diffusion and reaction details do not influence quantitatively the solution.

Those additional assumptions facilitate the construction of the transient model in two ways. They allow us to write differential equations for concentration fields that are smooth functions of position in the medium [the "smooth field approximation" (Jackson, 1977) is valid]; they uncouple the pore sturcture evolution problem from the diffusion and reaction problem. Of course, the properties of the porous solid still change spatially and temporally as the pore structure evolves, but locally they are determined completely by the conversion. Therefore, in the construction of the transient model, the properties of the pore structure, appearing in the mass and energy conservation equations, are assumed to be known functions of conversion or equivalently of porosity, since there is a linear relation between these two variables. These functions may be either an experimental result or provided by a theoretical model of the pore structure evolution, specifically a model that considers a bimodal pore-size distribution (e.g., Zygourakis et al., 1982). A similar pore structure was adopted by Hashimoto and Silveston (1973b) when they extended their probabilistic model so as to describe the diffusionally-controlled gasification. Since they considered concentration gradients in the small pores, however, they had to solve the pore structure evolution equations along with the intraparticle diffusion and reaction problem.

In the above discussion, it is understood that the char particles are considerably larger than the average macropore size so that effective transport and pore structure properties can be used for the macroporous network in the mathematical model. Since the average macropore size is quite large, however, this may not be the case for small particles, especially for particles in the pulverized fuel range. In this particle size range, the results of our model will be only qualitatively indicative of the actual transient behavior of the reacting char particles. For very small particles, the complete and rigorous analysis of the system may require not only simultaneous consideration of the pore structure evolution problem and of the diffusion and reaction problem but a very detailed analysis of the evolving pore structure.

Reactions, Rate Expression, and Model Parameters

Two heterogeneous reactions take place in the interior of the particle; the gasification of carbon by CO_2,

$$C + CO_2 \rightarrow 2CO, \text{ endothermic, } R1,$$

and the oxidation of carbon,

$$2C + O_2 \rightarrow 2CO, \text{ exothermic, } R2.$$

In the gas phase, the carbon monoxide is oxidized to CO_2 according to the reaction

$$2CO + O_2 \rightarrow 2CO_2, \text{ exothermic, } R3.$$

The homogeneous reaction is assumed to occur not only in the surrounding gas phase but also in the void space of the char particles. It is questionable whether this reaction, that proceeds via a radical mechanism (Howard et al., 1973), takes place in the interior of the particle. Several reports (e.g., Blackwood and McTaggart, 1959; Rosner and Allendorf, 1968) suggest a favored reaction of carbon with radical species similar to the ones involved in the homogeneous oxidation of CO. Therefore, radicals formed in the void space of the char particle may preferentially react with the carbon or be quenched at the solid surface. In a previous paper (Sotirchos and Amundson, 1984b), we investigated how the occurrence of the homogeneous reaction in the interior of the particle and the primarily produced amounts of CO_2 by reaction $R2$ (Arthur, 1951) influence the solution structure. Both effects were found to be significant only for large particles.

The reaction rate expressions used and the references in which they are reported appear in Table 1. However, developing the model we consider arbitrary rate expressions; hence it can be used with any other rate expressions. Since the rate expression of the homogeneous reaction contains the water vapor mole fraction, traces of water vapor are assumed to exist and to function only as a catalyst for the CO oxidation. The intrinsic reaction rates of the heterogeneous reactions, given on Table 1 per unit of internal surface area, can be easily expressed per unit of char volume at any level of conversion by the relation

TABLE 1. REACTION RATE EXPRESSIONS AND CONSTANTS

Reaction	Rate
$C + CO_2 \rightarrow 2CO$	$R_{s1} = k_1 \exp(-E_1/R/T)P_{x1}/T$, kmol CO_2/(m^2 int. surf. area·s)
(Dutta et al., 1977)	$k_1 = 5.301 \times 10^4$ kmol·K/m^2·s·atm $E_1 = 248.12 \times 10^3$ kJ/kmol
$2C + O_2 \rightarrow 2CO$	$R_{s2} = k_2 \exp(-E_2/R/T)Px_2$, kmol O_2/(m^2 int. surf. area·s)
(Smith, 1978)	$k_2 = 127.08$ kmol/m^2·s·atm $E_2 = 179.40 \times 10^3$ kJ/kmol
$2CO + O_2 \rightarrow 2CO_2$	$R_3 = k_3 \exp(-E_3/R/T)^{P2/T2} \times 2^{1/2} \times 3 \times H_2^{1/2}O$, O, kmol O_2/m^3·s
(Howard et al., 1973)	$k_3 = 9.667 \times 10^2$ kmol·K^2/m^3·s·atm^2 $E_3 = 125.6 \times 10^3$ kJ/kmol

$$R_{v\rho} = R_{s\rho} S_{gt} \rho_{po}(1 - \xi), \rho = 1,2, \tag{1}$$

where S_{gt} is the internal surface area at time t, corresponding to local conversion ξ, per unit of weight of unreacted solid (of initial composition).

The following expressions

$$\mathcal{D}_{ij}^e = \epsilon_M^2 \mathcal{D}_{ij} \tag{2a}$$

$$D_i^e = \epsilon_M^2 D_i \propto \epsilon_M^2 T^{1/2} \bar{r}_p M_i^{-1/2} \tag{2b}$$

are used for the estimation of the effective binary diffusion coefficients and Knudsen diffusion coefficients, respectively, and the thermal conductivity of the gas permeated porous matrix is assumed to be given by the expression

$$k^e = (1 - \epsilon_M)^2 k_m + \epsilon_M{}^2 k. \tag{3}$$

We use average values for the heat capacities of the gas mixture, $\bar{C}_{pg}$, and of the solid material, $\bar{C}_{ps}$, and the heat capacity of the porous solid, $\bar{C}_p^e$, expressed per unit of particle volume, is obtained from the relation

$$\bar{C}_p^e = (1 - \epsilon)\rho_B \bar{C}_{ps} + \epsilon c \bar{C}_{pg}. \tag{4}$$

To compute the transport and thermodynamic properties of the gas mixture that appear in the above expressions, we assume ideal gas behavior and we use an average local composition. Thus, based on the Chapman-Enskog equation the following approximate relations

$$\mathcal{D}_{12} = \mathcal{D}_{13} = \mathcal{D}_{14} = \mathcal{D} \tag{5a}$$

$$\mathcal{D}_{23} = \mathcal{D}_{34} = \mathcal{D}_{24} = \gamma \mathcal{D} \tag{5b}$$

$$c\mathcal{D} = (c\mathcal{D})^r \theta^{1/2}, \tag{5c}$$

with

$$\mathcal{D} = \mathcal{D}^r \frac{\theta^{3/2}}{\Pi},$$

are valid, while use of the Wilke equation and Eucken equation leads to the approximation

$$k = k^r \theta^{1/2}. \tag{6}$$

The variation of the reaction heats with the temperature will be given by the expression

$$(-\Delta H_\rho) = (-\Delta H_\rho)^o - \sum_i \nu_{i\rho} \bar{C}_{pi}(T - T^o). \tag{7}$$

The values of k and $c\mathcal{D}$ used in the calculations are computed at an average temperature, T_d, and an average value, $\bar{k}_m$, is also used for the thermal conductivity of the microporous solid. The latter was obtained by applying Eq. 3 to a set of data (Zamoluev et al., 1960) giving the thermal conductivity of heat-treated non-

TABLE 2. CHAR DATA, PHYSICAL DATA AND CONSTANTS, AND REFERENCE CONDITIONS AND PARAMETERS

$\rho_{po} = 340$ kg/m^3	$\epsilon \simeq \epsilon_M = 0.765$
$S_{go} = 27 \times 10^3$ m^2/kg	$\bar{k}_m = 1.891$ J/m·s·K
$W_b = 0.75$	$\bar{C}_{ps} = 1.458$ kJ/kg·K
$k^r = 6.58 \times 10^{-2}$ J/m·s·k	$(-\Delta H_1)^r = -1.74 \times 10^5$ kJ/kmol CO_2
$\mathcal{D}^r = 1.25 \times 10^{-4}$ m^2/s	$(-\Delta H_2)^r = 2.20 \times 10^5$ kJ/kmol O_2
$\gamma = 1.3$	$(-\Delta H_3)^r = 5.68 \times 10^5$ kJ/kmol O_2
$\bar{C}_{pg} = 39.77$ kJ/kmol·K	$\tilde{\epsilon} = 0.9$
$\sigma = 5.677 \times 10^{-11}$ kJ/m^2·s·K^4	
$T^r = 1{,}000$ K	$(\bar{r}_p)^r = 1{,}000$ Å
$p^r = 1$ atm	$T_d = 1{,}400$ K

caking Donets anthracite in the temperature range of interest. Values for the several transport and thermodynamic properties at the reference conditions and for the other physical parameters that appear in the above formulae are given on Table 2. As we have already mentioned, there is a linear relation,

$$\epsilon = \epsilon_o + (\epsilon_f - \epsilon_o)\xi, \tag{8}$$

between conversion and porosity. Therefore, the properties of the pore structure contained in the expressions giving the reaction rates per unit volume, Eq. 1, and the thermodynamic and transport properties of the porous solid can equivalently be considered functions of the total porosity.

The radiant interaction of the burning particle with the environment is assumed to be given by the single particle radiation scheme,

$$Q_R = \sigma\tilde{\epsilon}(T_s^4 - T_b^4) \tag{9}$$

which assumes that the particle interacts with an enclosure at ambient temperature. The physical parameters used in Eq. 9 are also given on Table 2.

Mathematical Model

We consider a porous, spherical char particle in an environment of CO_2, O_2, CO, and N_2, with the chemical species denoted by indices 1 to 4, respectively. Some water vapor may also exist, but it functions only as a catalyst in the oxidation of CO. The particle is surrounded by a stagnant boundary layer extending to radius b. In addition, we assume that the radius of the particle does not change as the combustion proceeds, that is, the ash layer does not peel off, and that the pressure variations have insignificant effects on the solution so that the total pressure can be considered constant. Then, the mass and energy balance equations are written, in general form, as

$$\epsilon c\frac{\partial x_i}{\partial t} + \nabla\cdot\boldsymbol{J}_i = \sum_{\rho=1}^{3}\nu_{i\rho}R_{v\rho} - x_i\Psi, \tag{10a}$$

$$\frac{\partial(\epsilon c)}{\partial t} + \nabla\cdot\boldsymbol{N} = \Psi, \tag{10b}$$

$$C_p^e\frac{\partial T}{\partial t} - \nabla\cdot(k^e\nabla T) + \sum_{i=1}^{4}\boldsymbol{N}_i\cdot(C_{pi}\nabla T) = \sum_{\rho=1}^{3}(-\Delta H_\rho)R_{v\rho}, \tag{10c}$$

where $R_{v3} = \epsilon R_3$,

$$\Psi = \sum_{j=1}^{4}\sum_{\rho=1}^{3}\nu_{j\rho}R_{v\rho}, \tag{10d}$$

and $R_{v\rho}$ is given by Eq. 1. The fluxes are related by the dusty gas model equations which for small pressure variations and negligible pressure buildup inside the particle are expressed as

$$\nabla x_i = \sum_{j=1,j}^{4}\frac{x_i\boldsymbol{N}_j - x_j\boldsymbol{N}_i}{c\mathcal{D}_{ij}^e} - \frac{\boldsymbol{N}_i}{cD_i^e}, \tag{10e}$$

where $\boldsymbol{N}_i = \boldsymbol{J}_i + x_i\boldsymbol{N}$. Equations 10 are valid not only in the interior of the particle but also in the boundary layer. In the boundary layer, $\epsilon = \xi = 1$, and only reaction $R3$ takes place so that the effective quantities used in the above formulae reduce, according to Eqs. 2, 3 and 4, to the respective quantities for the gas phase, and the dusty gas model equations take the familiar form of the Stefan-Maxwell relations.

TABLE 3. DEFINITIONS OF DIMENSIONLESS VARIABLES AND CONSTANTS

Symbol	Definition
ζ	r/a
β	b/a
θ	T/T^r
Π	P/P^r
λ	$N_i a/(c\mathcal{D})^r$
μ_i	$J_i a/(c\mathcal{D})^r$
β_i	$[(-\Delta H_i)^o c\mathcal{D}/k/T]^r$
γ_i	$E_i/R/T^r$
q_R	$Q_R a/k^r/T^r$
r_3	$R_3 a^2/(c\mathcal{D})^r$
r_{vi}	$R_{vi}a^2/(c\mathcal{D})^r$
r_{si}	$R_{si}a/(c\mathcal{D})^r$
δ_i	$(\mathcal{D}^e/D_i^e)^r$
Le_g	$\bar{C}_{pg}(c\mathcal{D}/k)^r$
Le_s	$\bar{C}_{ps}(c\mathcal{D}/k)^r M_C$
$Le(\theta,\epsilon)$	$\bar{C}_p^e\mathcal{D}^r/k^r$
Λ	$M_C c^r/\rho_{po}W_b$
τ	$t\mathcal{D}^r/a^2$
Φ_1^2	$k_1\exp(-\gamma_1)a^2(P/c\mathcal{D}/T)^r\rho_{po}S_{go}$
Φ_2^2	$k_2\exp(-\gamma_2)a^2(P/c\mathcal{D})^r\rho_{po}S_{go}$
Φ_B^2	$k_3\exp(-\gamma_3)a^2(P^2/c\mathcal{D}/T^2)^r x^{1/2}H_2O$
$f_1(\theta,\epsilon)$	$c\mathcal{D}^e/(c\mathcal{D})^r = \epsilon_M{}^2\theta^{1/2}$
$f_2(\theta,\epsilon)$	$(\mathcal{D}^e/D_i)/(\mathcal{D}^e/D_i)^r = \theta\bar{r}_p/(\bar{r}_p)^r$
$f_3(\theta,\epsilon)$	k^e/k^r
$f_4(\xi)$	$S_{gi}/S_{go}(1-\xi)$

In the interior of the particle one additional equation, for the carbon mass balance, is required, which in terms of the conversion is written

$$\frac{\partial\xi}{\partial t} = -\frac{M_C}{\rho_{po}W_b}\sum_{\rho=1}^{2}\nu_{C\rho}R_{v\rho}. \tag{11}$$

Three sets of boundary conditions and one set of initial conditions are required.

At $r = 0$:

$$\boldsymbol{N}_i = 0,\ \nabla T = 0.$$

At $r = a$:

$$\boldsymbol{N}_i^+ = \boldsymbol{N}_i^-,\quad x_i^+ = x_i^-,$$

$$T^+ = T^-,$$

$$-k^e(\nabla T)^- = -k(\nabla T)^+ + Q_R.$$

At $r = b$:

$$x_i = x_{ib},\quad T = T_b.$$

At $t = 0$:

$$x_i = x_{io},\quad T = T_o,\quad \xi = 0.$$

Considering an average heat capacity, $\bar{C}_{pg}$, for the gas mixture, using relations 1 to 8, rearranging the equations, and introducing dimensionless variables, the mathematical model is written as follows. The dimensionless variables, functions, and constants are given on Table III.

Model equations:

$0 \le \zeta < 1$ or $1 < \zeta \le \beta$:

$$\frac{\partial x_i}{\partial\tau} = F_i = \frac{\theta}{\epsilon}\left[-\frac{1}{\zeta^2}\frac{\partial}{\partial\zeta}(\zeta^2\mu_i) + \sum_{\rho=1}^{3}\nu_{i\rho}r_{v\rho} - x_i\Psi\right],$$

$$i = 1,\ldots 3, \tag{12a–c}$$

$$\frac{\partial\theta}{\partial\tau} = F_4 = \frac{1}{Le(\theta,\epsilon)}\left[\frac{1}{\zeta^2}\frac{\partial}{\partial\zeta}\left(\zeta^2 f_3(\theta,\epsilon)\frac{\partial\theta}{\partial\zeta}\right) - Le_g\lambda\frac{\partial\theta}{\partial\zeta} + \sum_{\rho=1}^{3}\beta_\rho r_{v\rho} - Le_g(\theta-\theta^o)\psi - Le_s(\theta-\theta^o)\sum_{\rho=1}^{2}\nu_{C\rho}r_{v\rho}\right], \quad (12d)$$

$$\frac{\partial\xi}{\partial\tau} = F_5 = -\Lambda\sum_{\rho=1}^{2}\nu_{C\rho}r_{v\rho}, \quad (12e)$$

$$0 = F_6 = -\frac{1}{\zeta^2}\frac{\partial}{\partial\zeta}(\zeta^2\lambda) + \psi + \frac{\epsilon}{\theta^2}F_4 - \frac{(\epsilon_f-\epsilon_o)}{\theta}F_5, \quad (12f)$$

where

$$r_{v1} = f_4(\xi)\Phi_1^2\frac{\Pi}{\theta}\exp\left[\gamma_1\left(1-\frac{1}{\theta}\right)\right]x_1, \quad (13a)$$

$$r_{v2} = f_4(\xi)\Phi_2^2\Pi\exp\left[\gamma_2\left(1-\frac{1}{\theta}\right)\right]x_2, \quad (13b)$$

$$r_{v3} = \epsilon r_3 = \epsilon\Phi_3^2\frac{\Pi^2}{\theta^2}\exp\left[\gamma_3\left(1-\frac{1}{\theta}\right)\right]x_2^{1/2}x_3, \quad (13c)$$

$$\psi = \sum_{j=1}^{4}\sum_{\rho=1}^{3}\nu_{j\rho}r_{v\rho}, \quad (13d)$$

$$\mu_1 = \frac{-f_1(\theta,\epsilon)\dfrac{\partial x_1}{\partial\zeta} - \delta_1\dfrac{f_2(\theta,\epsilon)}{\Pi}x_1\lambda}{1+\delta_1 f_2(\theta,\epsilon)/\Pi}, \quad (13e)$$

$$\mu_i = \frac{-\gamma f_1(\theta,\epsilon)\dfrac{\partial x_i}{\partial\zeta} - \gamma\delta_i\dfrac{f_2(\theta,\epsilon)}{\Pi}x_i\lambda + (\gamma-1)x_i\mu_1}{((\gamma-1)x_1+1) + \gamma\delta_i f_2(\theta,\epsilon)/\Pi}, \quad i = 2,3, \quad (13f,g)$$

$$\epsilon = \begin{cases}\epsilon_o + (\epsilon_f-\epsilon_o)\xi & \text{if} \quad 0 \le \xi < 1 \\ 1 \quad \text{if} \quad 1 < \zeta \le \beta.\end{cases} \quad (13h)$$

Boundary conditions:

At $\zeta = 0$:

$$\frac{\partial x_i}{\partial\zeta} = 0, \quad \frac{\partial\theta}{\partial\zeta} = 0, \quad \lambda = 0. \quad (14)$$

At $\zeta = 1$:

$$x_i^- = x_i^+, \quad \theta^- = \theta^+, \quad (15a,b)$$

$$\mu_i^- = \mu_i^+, \quad \lambda^- = \lambda^+, \quad (15c,d)$$

$$-\left[f_3(\theta,\epsilon)\frac{\partial\theta}{\partial\zeta}\right]^- = -\left[f_3(\theta,1)\frac{\partial\theta}{\partial\zeta}\right]^+ + q_R. \quad (15e)$$

At $\zeta = \beta$:

$$x_i = x_{ib}, \quad \theta = \theta_b. \quad (16a,b)$$

Initial conditions:

At $\tau = 0$:

$$x_i = x_{io}, \quad \theta = \theta_o, \quad \xi = 0. \quad (17a\text{-}c)$$

When it is assumed that the particle behaves isothermally, Eq. 12d for the interior of the particle, along with boundary condition 15e, is replaced by an overall energy balance at the surface of the particle which, in dimensionless form, is written

$$\left[\int_0^1 Le(\theta^-,\epsilon)d\zeta^3\right]\frac{d\theta^-}{d\tau} = 3\left[f_3(\theta,1)\left(\frac{\partial\theta}{\partial\zeta}\right)^+ - q_R\right] + \int_0^1\left[\sum_{\rho=1}^{3}\beta_\rho r_{v\rho} - Le_g(\theta-\theta^o)\psi - Le_s(\theta-\theta^o)\sum_{\rho=1}^{2}\nu_{C\rho}r_{v\rho}\right]d\zeta^3. \quad (18)$$

Computational Aspects

Spatial discretization of the model equations by spline collocation combined with temporal integration of the resulting equations is used for the solution of the mathematical model. The basis functions are constructed by techniques described by deBoor (1972, 1978), and the system of equations obtained after discretization is integrated in time by using a Gear-type method (Hindmarsh, 1976). The overall computation proceeds along the general lines of a method that was developed by Madsen and Sincovec (1976).

To reveal the pseudosteady-state structure underlying the transient paths, we also solve the pseudosteady-state problem at several times along each transient path. The pseudosteady-state model that results if one sets the time derivatives of concentrations and temperature in the general model equal to zero is a three-point boundary value problem (Sotirchos and Amundson, 1984b) and is solved by using a shooting method employing a Newton-Raphson iteration scheme. Some additional information regarding the numerical technique is given by Sotirchos (1982).

RESULTS AND DISCUSSION

The results we present here regard the effect of intraparticle thermal gradients and of the evolving char pore structure on the dynamic behavior of char particles burning in air at 1 atm pressure with 0.5% (mol/mol) water vapor present. The char properties used appear on Table 2. They were reported by Dutta et al. (1977) for the IGT Char No. HT155. The radiation scheme used throughout this study is the single particle scheme, Eq. 9, which is more suitable for a fluidized-bed combustor where the inert particles that surround and outnumber the burning char particles are essentially at ambient temperature. Also, the thickness of the boundary layer is fixed to one particle radius. The results are for char particles of uniform initial temperature in an inert atmosphere (N_2) which are introduced into the reactive environment at time $t = 0$.

The above type of char is a highly porous one with a relatively high ash content, about 25%, which partially justifies the assumption that the ash skeleton left after depletion of the combustible solid does not collapse. Since the char used is very porous, it will further be assumed that the macropores account for almost all the porosity at any level of conversion and that the Knudsen diffusion terms used in the dusty gas model equations can be neglected. Note that our calculations have shown (Sotirchos and Amundson, 1984a) that if the pore-size distribution of the char sample, Table 2, were narrow and unimodal, the initial average pore radius should be about 1,700 Å.

With the additional assumptions stated above, the evolution of the pore structure is basically determined by the dependence of the specific internal surface area on the conversion. The latter is given implicitly by the dependence of the heterogeneous reaction rate ratio (reaction rate at conversion ξ over reaction rate at conversion zero), $f_4(\xi)$, on the conversion. Two qualitatively different reaction rate ratio vs. conversion curves, which are reported for the IGT Char No. HT155 are used (Figure 1); namely, that obtained by Dutta et al. (1977) from experiments with CO_2 (the ratio is a monotonically decreasing function of conversion, pattern $P1$) and by Dutta and Wen (1977) from experiments with O_2 (the heterogeneous reaction rates go through a maximum, pattern $P2$). Since the above investigators determined the function $f_4(\xi)$ indirectly by measuring the reaction rates at several conversion levels, it is not surprising that each series of experiments led to a different curve. Perhaps some micropores accessible to O_2 were not accessible to the larger CO_2 molecules, and inorganic impurities present in the ash catalysed the reactions differently. However, in our study the internal surface area is considered equally accessible to both reactants. The value for the internal surface area which appears on Table 2 is the portion of the total surface area that was considered accessible to CO_2 (Dutta et al., 1977).

Initial Pseudosteady-State Structure

The initial pseudosteady state structure of the problem for two particle sizes is depicted in Figure 2 in terms of the center and

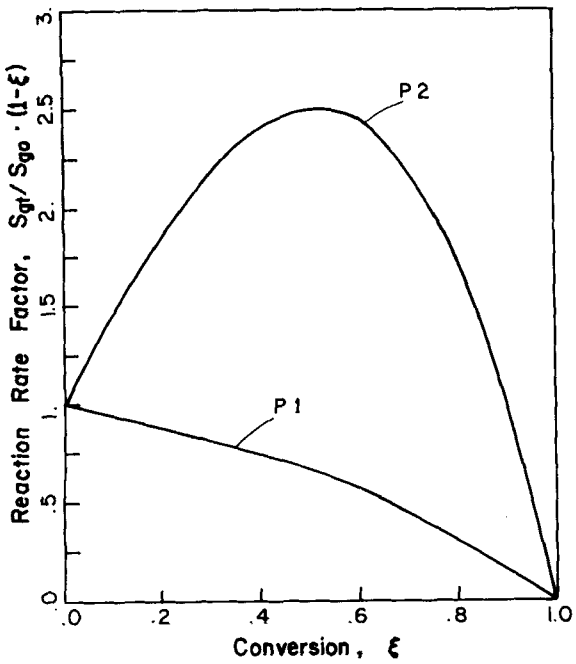

Figure 1. Dependence of the heterogeneous reaction rates per unit volume on the conversion for the two patterns of pore structure evolution.

surface temperature or of the isothermal particle temperature dependence on the ambient temperature. The pseudosteady-state problem at $t = 0$ has been studied extensively by Sotirchos and Amundson (1984b), and the reader may consult this publication for further details. However, knowledge of the initial pseudosteady-state (PSS) structure of the problem will enable us to determine *a priori* the possible qualitative effects of the several assumptions and simplifications on the transient behavior of the system, and it will facilitate the explanation of the actual dynamic behavior of the burning particles.

Thus, according to the results of Figure 2, consideration of thermal gradients modifies the initial PSS structure basically in two ways; it enlarges the region of multiple solutions and shifts the ignition temperature, the ambient temperature value beyond which only the upper ignited branch of the solution exists, to lower temperatures. Therefore, there is a large region of ambient temperature in which nonisothermal particles may sustain ignition as the upper branch of the solution is present while the respective isothermal particles will suffer extinction and approach the unignited branch of the solution. Also, for the practically more interesting case of particles with initial temperatures close to or lower than the ambient value, there is a region of ambient temperature

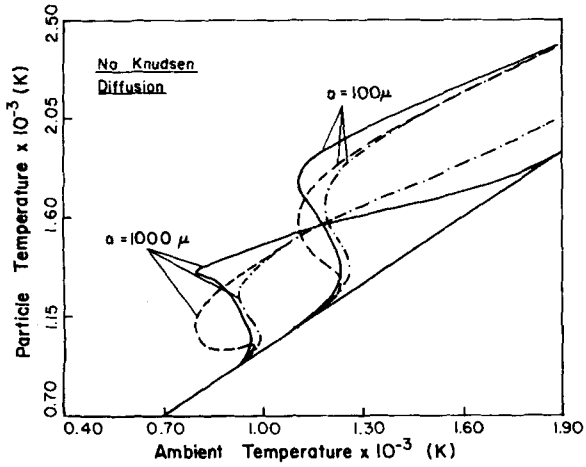

Figure 2. Pseudosteady-state loci at $t = 0$. —: center temperature, - - -: surface temperature, -.-.-: isothermal particle temperature.

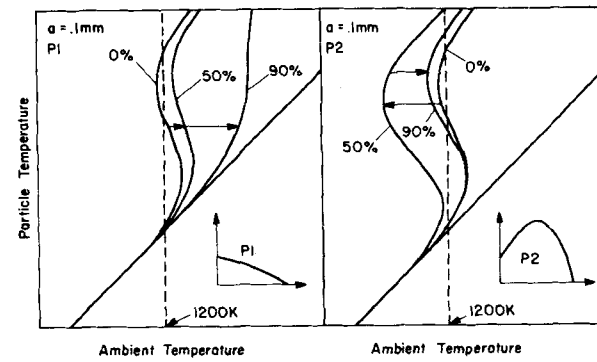

Figure 3. Effect of uniform conversion changes on the isothermal particle solution locus.

in which the nonisothermal particles find themselves in the ignition regime of the initial pseudosteady state structure and consequently may ignite. On the contrary, in the very same region the isothermal pseudosteady-state model still predicts the unignited branch of the solution. The initial PSS structure of the problem, therefore, forecasts significant qualitative and quantitative effects of intraparticle thermal gradients on the transient behavior of the system, especially in the neighborhood of the multiplicity region. However, there may be differences in a much wider temperature region since the PSS solution locus shifts as the combustion proceeds (Figure 3).

Unfortunately, since both patterns of pore structure evolution start from the same initial conditions (the same PSS structure), the initial PSS structure cannot provide any information for the possible effects of the evolving char pore structure on the solution. This can be deduced only from the underlying transient paths of the PSS structure. At a certain conversion level, however, the solution of the pseudosteady state problem requires knowledge of the conversion profile which can be obtained only from the solution of the transient problem. Thus, in order to investigate a priori the underlying transient paths of the PSS structure, one must assume that the conversion changes in a specific manner; for example, uniformly throughout the particle.

The effect of the two patterns of pore structure evolution on the isothermal particle PSS locus for uniform changes of conversion is given in Figure 3. The $P1$ model locus (Figure 3a) unfolds progressively to the right as the conversion increases, the ignition temperature becomes higher, and the multiplicity region shrinks. At 90% conversion level, $T_p(T_b)$ is a monotonically increasing function. The $P2$ PSS locus, on the other hand, folds progressively to the left up to about 50% conversion, the ignition temperature takes on lower values, and the multiplicity region becomes larger. Beyond this conversion level, however, the T_p vs. T_b locus given

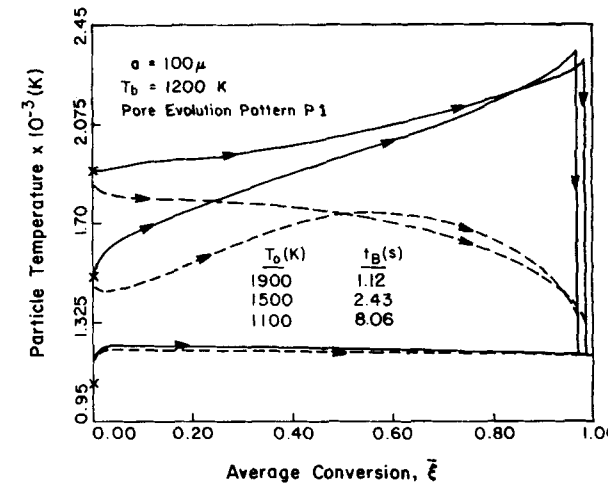

Figure 4. Temperature histories of a non-isothermal particle. —: center temperature, - - -: surface temperature.

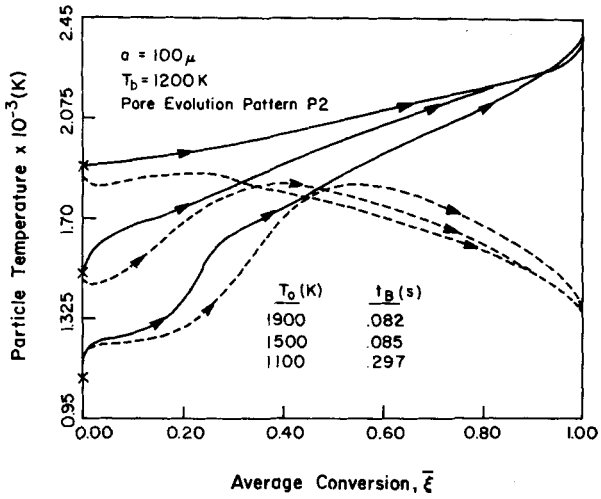

Figure 5. Temperature histories of a non-isothermal particles. See Figure 4.

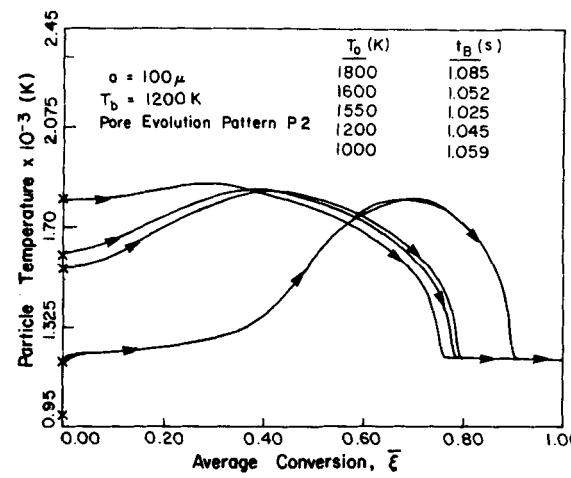

Figure 7. Temperature histories of an isothermal particle.

by the $P2$ model starts behaving like the $P1$ model locus; that is, it shifts continuously to the right.

Thus, particles that start reacting in the multiplicity region of the initial pseudosteady-state structure along the ignited branch of the solution will remain ignited at much higher levels of uniform conversion if their pore structure evolves according to pattern $P2$. For example, at 1,200 K, a $P1$ particle will suffer extinction at about 25% conversion, while a $P2$ particle will be ignited even at 90% conversion level. Also, even though a $P1$ particle that starts reacting along the unignited branch of the solution never ignites, a $P2$ particle that burns along the unignited steady state branch at ambient temperatures higher than 1,150 K will find itself inside the ignition regime after a certain conversion level, and hence it may ignite. For instance, a $P2$ particle at 1,200 K may ignite beyond 35% conversion. Similar conclusions are also drawn from a graph, analogous to Figure 3, for the nonisothermal version of the model. Therefore, the two patterns of pore structure evolution will influence strongly the dynamic behavior of the system. The quantitative effects will be, of course, different from what the approximate PSS structure reveals, but the qualitative effects must be similar.

Transient Paths and Underlying PSS Structure

To make the several transient paths comparable, we have chosen to plot temperatures representative of the intraparticle temperature profile (center and surface temperature or isothermal particle temperature) as functions of the average conversion rather than as functions of time (Figures 4 to 11). The 99% burn-off time, t_B, for each initial temperature also appears in the figures. The temperature histories of burning nonisothermal particles (Figures 4, 5, 8 and 9) show that when a particle is in an ignited state, the difference between its center (solid curves) and surface temperature (broken curves) becomes very high at high levels of conversion. This is expected because at high conversion levels the thermal conductivity of the gas permeated solid matrix is very low, actually the effective thermal conductivity of the ash skeleton. Also, the computations have shown that at ambient temperatures lying in the multiplicity region of the initial pseudosteady-state structure, there is a critical value of initial temperature above which a particle ignites. Particles with initial temperatures lower than this value are quenched, but they might ignite at higher conversion levels. Because of the thermal inertia of the particle and the fact that the PSS structure evolves differently for each pattern of pore structure evolution, this critical temperature value is not the same for both patterns at a given ambient temperature. Specifically, it is lower for particles with pore structure evolving according to pattern $P2$. Although the relative position of the critical initial temperature varies with the ambient value of temperature, this critical value lies close to the average temperature of the intermediate steady state, usually higher than the latter.

Another general observation for $P1$ particles, isothermal and nonisothermal, is that they do not ignite as soon as they move into the ignition regime of the initial PSS structure. Since the upper-bound of the multiplicity region moves to the right as the combustion proceeds (Figure 3a) and the particle is heated by consuming itself, it may be found again inside the current multiplicity region and be quenched if its average temperature is not high enough. Thus, the actual ignition temperature of a $P1$ particle with low initial temperature is higher than the value predicted by the initial PSS structure. A similar phenomenon was observed in the

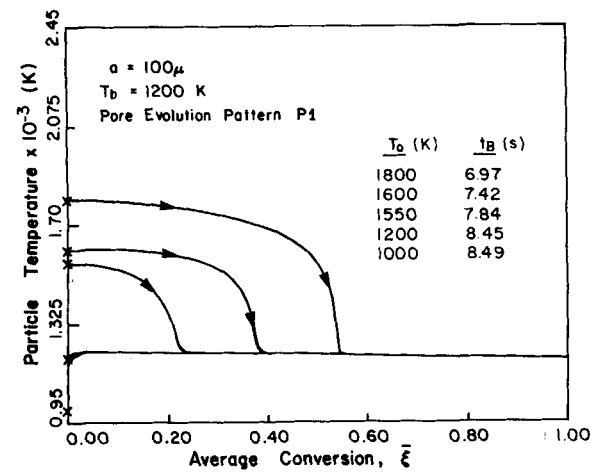

Figure 6. Temperature histories of an isothermal particle.

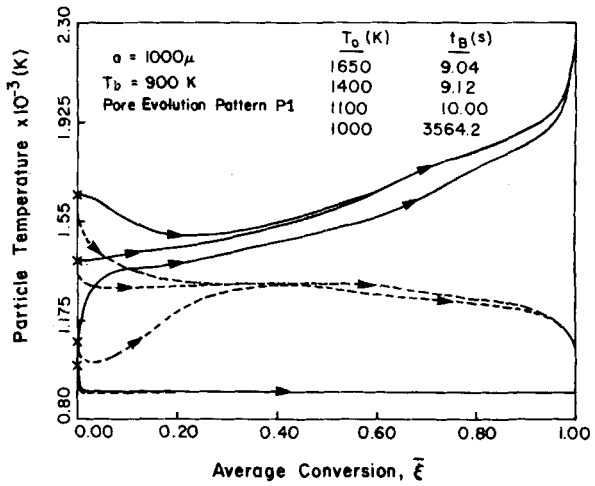

Figure 8. Temperature histories of a non-isothermal particle. See Figure 4.

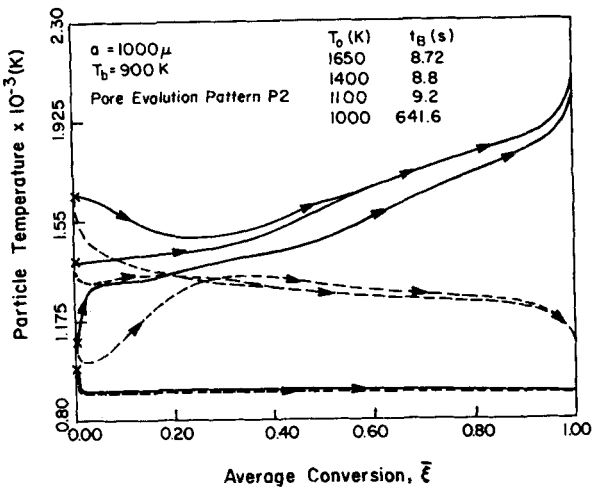

Figure 9. Temperature histories of a non-isothermal particle. See Figure 4.

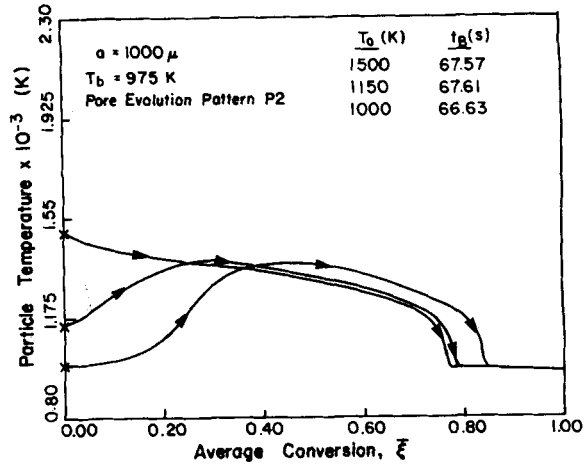

Figure 11. Temperature histories of an isothermal particle.

study of the regeneration of coked catalyst particles (Sotirchos et al., 1983). However, this is not true for $P2$ particles.

Figures 4 and 5 give the transient paths followed by a 0.2 mm (diameter) nonisothermal char particle with several initial temperatures and pore structure evolving according to patterns $P1$ and $P2$, respectively. The initial temperatures of 1,900 and 1,500 K are higher than the critical initial temperature of each case, which lies close to the average temperature of the intermediate steady state in Figure 2 (about 1,410 K), and therefore the particles ignite. The transient paths are qualitatively similar up to high levels of conversion beyond which the $P1$ particles suffer extinction (Figure 4). The center temperature of the particles starts to increase rapidly, but suddenly it drops to the ambient value. It is remarkable that the same behavior was exhibited by spheres (1.25 cm in diameter) of porous carbon in the experiments of Kurylko and Essenhigh (1973). Since different starting temperatures lead to dissimilar conversion profiles, $P1$ particles of different initial temperatures do not suffer extinction at the same value of average conversion. However, it is not always true that the particle of higher initial temperature is quenched at higher conversions. Unlike distributions of conversion yield different profiles of pore structure properties. The conversion at which the particle suffers extinction depends on the combined effect of the above profiles on the pseudosteady state structure, but the case that appears in Figure 4 is the most favored one. For nonisothermal particles burning according to pattern $P2$, our results show that extinction takes place only at very high conversion, beyond the 99% conversion level, when all the reactive material has practically been depleted. This different behavior is probably caused by the higher heterogeneous reaction rates at high local conversions in pattern $P2$ (Figure 1).

Particles of low initial temperature (1,100 K) approach the unignited branch of the solution in both cases (Figures 4 and 5). The $P1$ particle follows the unignited branch up to complete conversion, but the $P2$ particle apparently moves into the ignition regime of the PSS structure at about 0.15 conversion and ignites. Because of its thermal inertia, however, its ignition is not instantaneous. The burning time of the $P1$ particle at 1,200 K is almost equal to the kinetic control limit, and most of the burning time shown in Figure 5 is spent by the $P2$ particle on the lower unignited branch. Also, the ignited $P1$ particles of Figure 4 spend only a fraction of their lifetime in an ignited state. This time is comparable to the burning time of the respective $P2$ particles (Figure 5), which is close to the diffusion control limit.

Some isothermal particle results are shown in Figures 6 and 7. Particles with pore structure evolving according to $P1$ pattern (Figure 6) and initial temperatures higher than but close to the temperature of the intermediate steady state (1,540 K) of the initial PSS structure (Figure 2) do not ignite. Thus, particles with 1,550 and 1,600 K initial temperature remain in an ignited state for some time but never reach the upper ignited branch of the solution. As the approximate pseudosteady state results show (Figure 3a), at a given ambient temperature the intermediate steady state moves upwards merging with the upper steady state, and consequently the above particles are found between the intermediate and the unignited steady state after some conversion. Actually, only the $P1$ particle with T_o = 1,800 K ignites, but it also suffers extinction when the ignited branch vanishes.

It is interesting to observe that at low or high levels of conversion all isothermal particles suffer extinction. This behavior chiefly causes all the quantitative differences between the two versions of the model, isothermal and nonisothermal. As we have already pointed out in the study of the pseudosteady-state problem (Sotirchos and Amundson, 1984b), a particle that is considered to behave isothermally, loses heat by radiation and conduction at higher temperatures than a nonisothermal particle of similar average temperature. Particularly, the latter loses heat at a progressively lower temperature because its thermal conductivity decreases rapidly with conversion. Thus, the initial ignition of the isothermal particles in Figures 6 and 7 does not have any dramatic effect on the predicted burning times, as eventually the particles spend most of their lifetime in the kineticlly-controlled regime. As Figure 7 indicates, the lower the initial temperature, the higher the conversion level at which extinction of the particles takes place. However, since there are several other factors that influence the PSS structure of the solution and the thermal inertia of the particle, which actually determine the extinction conversion of the particle, the above phenomenon is not always the observed one. As Figure 10 shows, it may also happen for $P1$ particles.

Transient paths for a larger particle (2 mm) at 900 K are shown in Figures 8 and 9. Since the ambient ignition temperature never

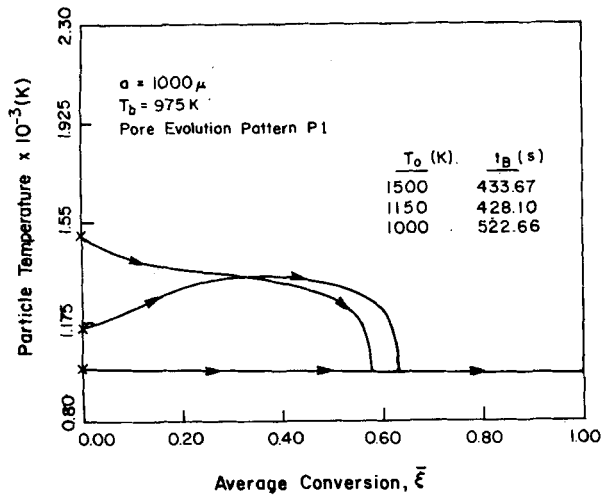

Figure 10. Temperature histories of an isothermal particle.

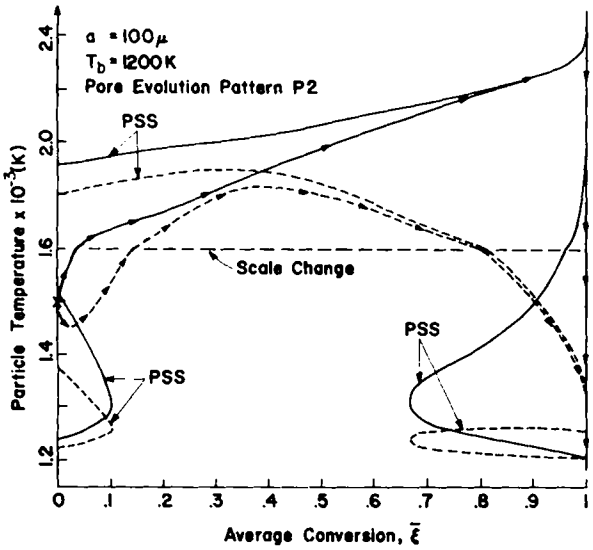

Figure 12. Transient path and underlying PSS structure of a non-isothermal particle. The arrows indicate the transient trajectories; —: center temperature, - - -: surface temperature.

takes on a value lower than 900 K, even the $P2$ particle that starts following the unignited branch never ignites. The burning times of the ignited particles are close to the diffusion control limit which depends on the particle radius only. For a given initial temperature, the difference between the burning times of ignited $P1$ and $P2$ particles is less than 8%. As expected, the kinetic control burning time given by pattern $P2$ is lower, because the predicted heterogeneous reaction rates per unit volume are higher at any conversion level (Figure 1). At intermediate conversion levels (Figures 4 and 5), the ignited $P2$ particles present smaller temperature differences between center and surface. As the $P2$ particles become more reactive to oxygen at higher local conversions, the penetration depth of oxygen into the unreacted core is very small, and thus, in this region only the reduction of CO_2 occurs to any extent.

Figures 10 and 11 give some results for large isothermal particles at 975 K. For particles with pore structure evolving according to pattern $P2$, the results are qualitatively similar to those of Figure 7. At this temperature, however, the ignited branch of the PSS solution for $P1$ particles does not vanish at very low levels of conversion. Thus, a $P1$ particle with 1,150 K initial temperature ignites although the temperature of the intermediate steady state at t = 0 (about 1,110 K, Figure 2) is not much smaller.

The specific transient trajectory followed by a particle can be fully explained only by considering the underlying PSS structure.

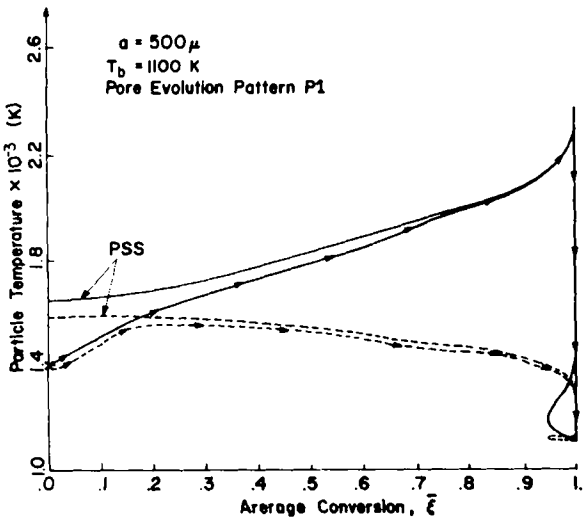

Figure 13. Transient path and underlying PSS structure of a nonisothermal particle. See Figure 12.

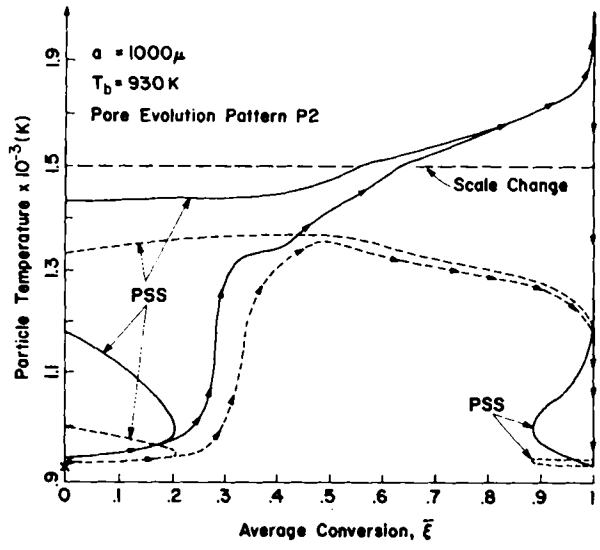

Figure 14. Transient path and underlying PSS structure of a nonisothermal particle. See Figure 12.

This obtains easily if one introduces in the pseudosteady state model developed previously (Sotirchos and Amundson, 1984b) the conversion profiles given by the transient model at several times along the transient trajectory or equivalently at several average conversion levels. Thus, Figure 12 presents the transient trajectories and the underlying PSS structure for a 0.2 mm particle at 1,200 K with pore structure evolving according to pattern $P2$. The initial temperature (1,500 K) is higher than the critical ignition temperature, and the particle ignites. The two lower branches disappear at about 0.11 conversion, they reappear at 67% conversion, but the particle still follows the ignited branch, as the latter is always present. Figure 13 presents a qualitatively similar case in which a $P1$ particle starts reacting in the ignition regime of the initial PSS structure. Indeed, the particle approaches the only branch present and follows it up to complete conversion. The two lower branches appear in the PSS solution at high conversion levels, but the upper ignited one is always present.

Figure 14 investigates the opposite phenomenon for a large (2 mm) particle at 930 K. The particle starts following the unignited branch which at 0.21 conversion vanishes merging with the intermediate branch. Then, the particle moves towards the only remaining solution branch, the ignited one, and starts burning along it. The two lower branches reappear at 88% average conversion, but since the upper branch still exists, the particle remains ignited.

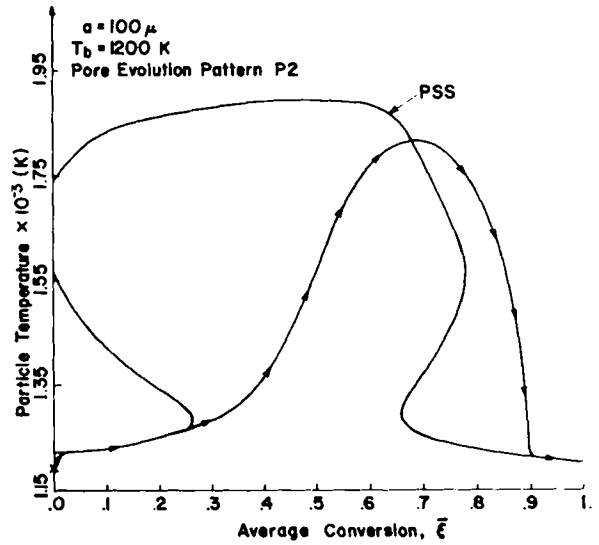

Figure 15. Transient path and underlying PSS structure of an isothermal particle. The arrows indicate the transient trajectory.

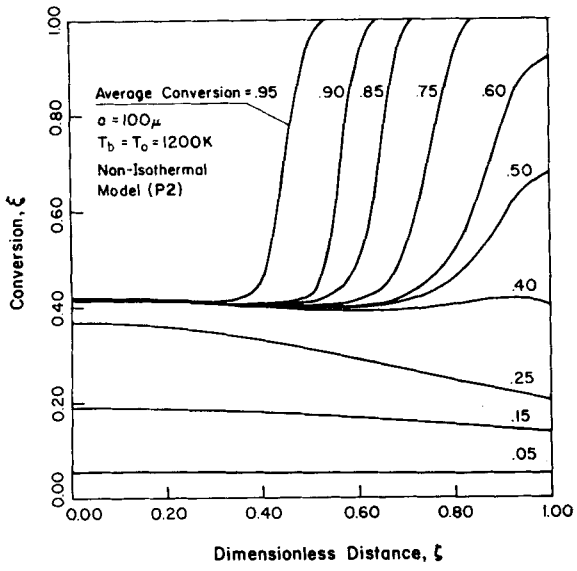

Figure 16. Conversion profiles at various levels of average conversion.

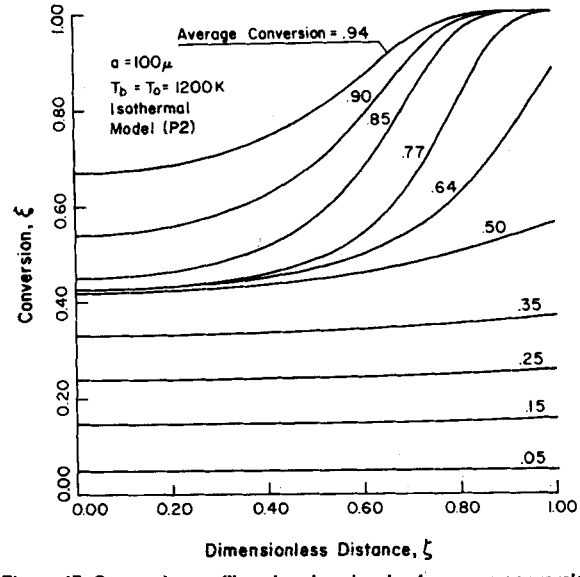

Figure 17. Conversion profiles at various levels of average conversion.

A similar but more interesting behavior exhibited by isothermal $P2$ particles in Figure 7 appears in Figure 15. The particle initially burns along the unignited branch which, however, ceases to exist at 28% conversion. Then, the particle moves towards the only remaining upper ignited steady state solution. However, when it eventually attains high temperatures, the ignited branch starts to approach the intermediate steady state solution, which has in the meantime reappeared along with the unignited branch at about 0.65 conversion level. Finally, the two upper branches merge together and vanish, and only the unignited branch continues to exist. The particle then falls to the unignited branch and follows it up to complete conversion.

Some conversion profiles at several average conversion levels are presented in Figures 16 and 17. Both figures correspond to the most interesting combustion behavior observed, where a burning particle follows successively the unignited and the ignited branches of the solution. Thus, the results of Figure 16 are representative of the combustion behavior of the $P2$ particle in Figure 5 with low initial temperature. Up to 0.15 conversion, the process is kinetically controlled, and almost uniform changes of conversion are observed. However, the conversion is higher in the region close to the center, since the effect of the higher center temperature on the reaction rates is stronger than the unfavorable effect of the lower reactant (O_2) concentration. In the time interval that corresonds to conversions between 0.15 and 0.40 the char particle moves towards the ignited branch of the solution, and we still observe conversion changes throughout the particle. However, when the particle reaches the upper ignited branch, the conversion profile moves as a sharp front towards the center of the particle. The combustion process is diffusionally controlled, and no significant conversion changes occur in the inner core of the particle.

Similarly, the isothermal particle of Figure 17 follows the unignited branch up to about 30% conversion (Figure 14). Indeed, the conversion is the same throughout the particle. Actually, it is slightly higher close to the surface because of higher oxygen concentration in this region. Between 0.30 and 0.50, the particle ignites and approaches the ignited branch. The conversion still changes significantly in the whole intraparticle region, but more intensely close to the surface. Between 0.50 and 0.80 average conversion, the process is almost diffusionally controlled, and the conversion does not change noticeably close to the center. At 80% conversion the particle returns to the kinetically controlled region, and again the conversion starts to change everywhere.

Although the cases shown in Figures 16 and 17 are very general, they do not cover all the possible patterns of conversion change observed. Thus, a very interesting behavior is shown in Figure 18 which depicts the conversion profiles of a $P1$ particle whose trajectory appears in Figure 8. As the porosity of the particle increases, the intraparticle temperature differences become larger, and thus the reactive material next to the surface of the particle is at progressively lower temperatures. After some average conversion level the local conversion takes on higher values at the surface than in the inner core, and the particle becomes considerably less reactive (Figure 1) close to its surface (pattern $P1$). Because of the above two reasons, the combustion rate profile presents a maximum in the interior of the particle. Thus, the carbon is depleted at some radial distance while there is still some combustible solid left close to the surface. However, the part of the conversion profile between the center and the point where depletion of carbon has occurred moves as a sharp front towards the center of the particle with increasing average conversion. Since the local reactivity of a $P2$ particle takes on low values only at very high conversions, the above phenomenon is less pronounced for $P2$ particles and not very common. The possibility of having such a situation, as shown in Figure 18, must be taken into account when disintegration of the solid structure at high conversion levels is considered.

Structure of the Burning Time

Most of the results presented above are summarized in Figures 19 and 20 which give the burning time structure in terms of the dependence of the 99% conversion time, t_B, on ambient temperature and particle size for both isothermal and nonisothermal $P1$ or $P2$ particles. The results given are for the most interesting, from a practical point of view, cases where the initial particle temperature is lower than or close to the ambient value. Particularly, in order to reduce the number of parameters, we have considered particles with initial temperatures equal to the ambient temperature. At a given ambient temperature, however, the results are directly applicable to any particle with initial temperature below the ignition limit, since the particles reach the unignited branch within a small fraction of the 99% combustion time.

As it is expected from the burning paths presented, the isothermal model predicts higher burning times than its nonisothermal version. However, the difference of their predictions is practically significant mostly in the transition regime, in which both kinetics and intraparticle diffusion are important, where in some cases it is greater than one order of magnitude. Thus, for a given pore structure evolution pattern the fixed particle radius (Figure 19), the burning times predicted by both versions of the model almost coincide at low ambient temperatures with the kinetic control asymptote (broken straight lines). As we increase the ambient temperature, the nonisothermal particle ignites, and a sharp decrease

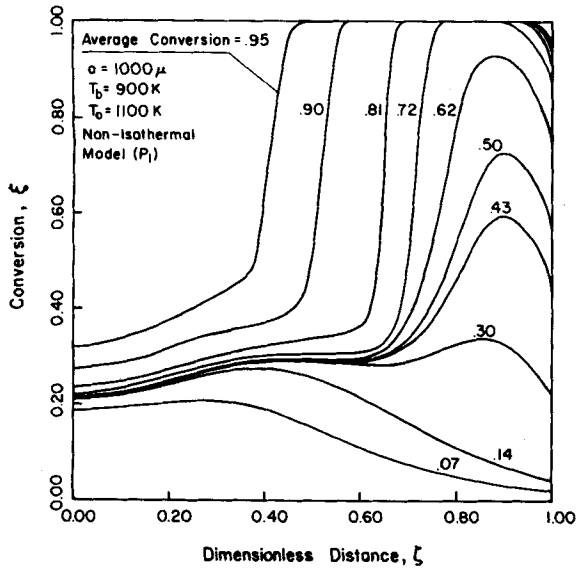

Figure 18. Conversion profiles at various levels of average conversion.

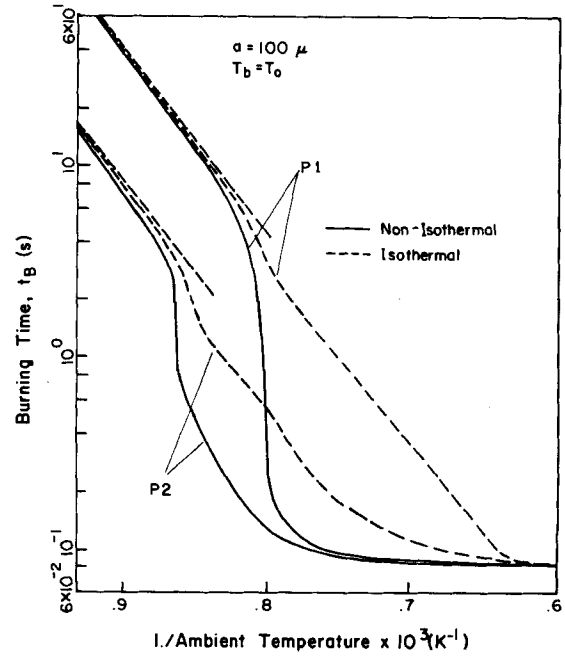

Figure 19. Dependence of burning time on ambient temperature.

in the computed burning time is observed, while the combustion process of the isothermal particle is still kinetically controlled. At higher ambient temperatures the isothermal particle also ignites, but since it suffers extinction at some conversion level, the decrease in the burning time is neither sharp nor as large as for the nonisothermal particle. The burning time given by each model continues to decrease with increasing ambient temperature, and at very high temperatures all cases exhibit similar burning times, approaching the diffusion control limit that is independent of the temperature. Since the isothermal particles always suffer extinction at some conversion, there is some material left that has to be burned out in the kinetically-controlled regime. As a result, the isothermal particle curves stay almost parallel to the kinetic control asymptotes and approach the diffusion control limit at the point where this becomes comparable to the respective kinetic control burning time.

The burning time behaves similarly as we change the radius of the particle keeping the value of ambient temperature constant (Figure 20). However, the kinetic control burning time is constant, while the diffusion control burning time varies proportionally to the square of the particle radius. Therefore, in each case there is an optimum value of particle radius that gives minimum burning time. This optimum value is well defined for the nonisothermal model, but for the isothermal version there is a whole range of particle radii that gives burning times close to the optimum. Again, observe that the isothermal particle curves start to approach the diffusion control limit after the point where the kinetic control asymptote meets the latter. Probably, this structure of the burning time vs. particle radius relation is the main reason that theoretical predictions of the burning times of small particles based on a diffusion control assumption—which is true for large particles—are much smaller than the experimentally observed values (Ross and Davidson, 1982).

The two patterns of pore structure evolution predict similar burning times at the limit of diffusion control but different kinetic control burning times. As we have already seen, Figures 8 and 9, pattern $P2$ predicts lower burning times in the kinetically-controlled regime because its heterogeneous reaction rates are higher at any conversion level (Figure 1). In the transition regime the $P2$ particles ignite after spending some time in the kinetically-controlled region, at ambient temperatures lower than the ignition limit of the initial pseudosteady-state structure. The burning time of a $P2$ particle approaches the limit of diffusion control only when the particle moves into the ignition regime of the initial ($t = 0$) PSS structure. The $P1$ particles, on the other hand, ignite only at ambient temperatures of the ignition regime. Actually, their ignition limit is higher than the upperbound of the initial multiplicity region, because of the thermal inertia of the particle. Therefore, in addition to the kinetically-controlled regime there is a relatively wide region of ambient temperature in which the predictions of the two different patterns of pore structure evolution differ substantially, in some cases by almost two orders of magnitude. The differences for the isothermal particle results are not so large, but they are observed in a much wider region, about 400 K.

It is very interesting to observe that close to the ambient temperature corresponding to the ignition limit of the initial PSS locus for the isothermal particle not only the $P1$ isothermal particle curve but also the respective $P2$ curve changes slope (Figure 19). As the simulation results have shown, at ambient temperatures lower than the ignition limit of the initial PSS locus, the isothermal $P2$ particle returns, after ignition, to the unignited branch of the solutions at progressively lower conversion levels as the ambient temperature increases. However, when the $P2$ particle enters the ignition regime, the conversion at which it suffers extinction starts to increase again, thus causing the slope of the t_B vs. $1/T_b$ curve to change.

Similar conclusions, regarding the effect of the pattern of pore structure evolution, can be drawn from the t_B vs. radius curves (Figure 20). Again, the $P1$ particle ignites only for particle radii greater than the ignition radius of the initial PSS structure, while the $P2$ particles ignite for lower values of particle radius after spending some of their lifetime in the kinetically-controlled region.

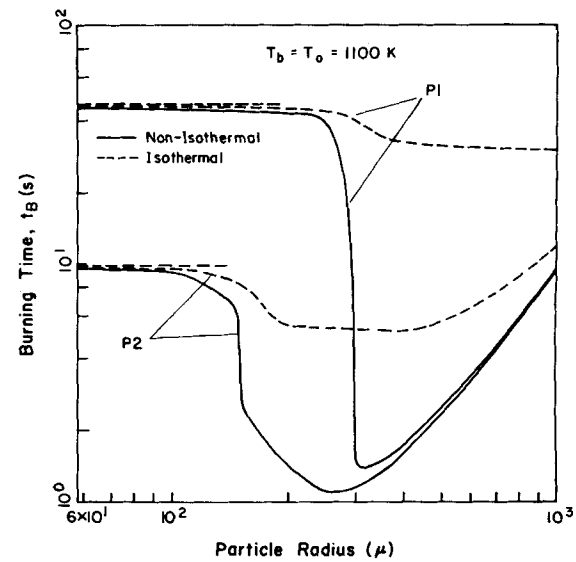

Figure 20. Dependence of burning time on particle radius.

For other values of particle radius and at other ambient temperatures, there may be some local differences in the structure of the burning time, but the general picture is similar. Thus, increasing the particle radius in Figure 19 moves the curves up and to the left with the same kinetic control asymptotes. On the other hand, decreasing the ambient temperature in Figure 20 moves all curves up and to the right while the diffusionally-controlled limit remains the same.

ACKNOWLEDGMENT

The early phase of this work was supported by the Department of Energy. The major portion, however, was supported by the University of Houston with major grants for computer time and stipends.

NOTATION

Symbols that do not appear here and definitions of dimensionless quantities are given on Table 3.

a = particle radius, m
b = distance from the center up to the external edge of the boundary layer, m
c = gas mixture concentration, kmol/m^3
$\overline{C}_{pi}, \overline{C}_{pg}$ = average heat capacities of the ith species and of the gas mixture, respectively, kJ/kmol·K
$\overline{C}_{ps}$ = average heat capacity of the solid, kJ/kg·K
$\overline{C}_p^e$ = effective heat capacity of the porous matrix, kJ/m^3·K
D_i, D_i^e = Knudsen and effective Knudsen diffusion coefficient, respectively, m^2/s
$\mathcal{D}_{ij}, \mathcal{D}_{ij}^e$ = binary and effective binary diffusion coefficient of the i-j pair, respectively, m^2/s
E_i = activation energy of the ith reaction, kJ/kmol
H_i = molar enthalpy of the ith species, kJ/kmol
J_i = molar flux of the ith species relative to the molar-average velocity, kmol/m^2·s
k, k^e, k_m = thermal conductivity of the gas mixture, of the porous solid, and of the microporous solid, respectively, kJ/m·s·K
k_i = frequency factor of the ith reaction, Table 1
Le_g = Lewis number of the gas phase
$Le_s, Le(\theta,\epsilon)$ = modified Lewis numbers for the solid, Table 3
M_i = molecular weight of the ith species, kg/kmol
N, N_i = total molar flux and molar flux of the ith species, respectively, kmol/m^2·s
P = pressure, atm
Q_R = radiation flux, kJ/m^2·s
r = radial coordinate, m
r_p = pore radius, m
R = gas constant, m^3·atm/kmol·K
R_{si}, R_{vi} = reaction rate of the ith reaction per unit of internal surface area and per unit of particle volume, respectively, Table 1
R_3, R_{v3} = reaction rate of the homogeneous reaction per unit volume and per unit of particle volume, respectively, Table 1
S_{go}, S_{gt} = available internal surface area at time zero and t, respectively, m^2/kg
t = time, s
T = temperature, K
T_d = temperature used in the calculation of average physical properties, K
T_p = isothermal particle temperature, K
V_p = volume of particle, m^3
W_b = initial carbon content of the char sample, kg/kg
x_i = mole fraction of the ith species

Greek Letters

β_i = dimensionless heat of the ith reaction
γ = defined in Eq. 5
γ_i = dimensionless activation energy of the ith reaction
$(-\Delta H_i)$ = heat of the ith reaction, kJ/kmol
ϵ, ϵ_M = total porosity and macropore porosity, respectively
ϵ_f = porosity of the ash layer $(= W_b + \epsilon_o(1 - W_b))$
$\bar{\epsilon}$ = emissivity of carbon
ζ = dimensionless distance
θ = dimensionless temperature
λ = dimensionless molar flux
μ_i = dimensionless molar flux relative to the molar-average velocity
$\nu_{i\rho}$ = stoichiometric coefficient of the ith component in the ρth reaction
ξ = conversion
Π = dimensionless pressure
ρ_B = true density of the solid $(= \rho_{po}/(1 - \epsilon_o))$, kg/m^3
ρ_{po} = density of carbon particle at time zero, kg/m^3
σ = Stefan-Boltzmann constant, kJ/m^2·s·k^4
τ = dimensionless time
Φ_i = modified Thiele modulus of the ith reaction
ψ = defined by Eq. 13d
Ψ = defined by Eq. 10d

Subscripts

c, s, b = refer to values at the center, at the surface, and at the edge of the boundary layer, respectively
1 = refers to CO_2 or to its reaction with carbon
2 = refers to O_2 or to its reaction with carbon
3 = refers to CO or to its reaction with O_2
4 = refers to N_2
o = refers to initial values

Superscripts

$-, +$ = refer to values at $r = a$ before and after the surface of the particle, respectively
o = refers to values computed at temperature T^o
r = refers to values computed at the reference conditions, Table 2

LITERATURE CITED

Arthur, J. R., "Reaction Between Carbon and Oxygen," *Trans. Faraday Soc.*, **47**, p. 164 (1951).

Bhatia, S. K., and D. D. Perlmutter, "A Random Pore Model for Fluid Solid Reactions: I. Isothermal, Kinetic Control," *AIChE J.*, **26**, p. 379 (1980).

Bhatia, S. K., and D. D. Perlmutter, "A Random Pore Model for Fluid Solid Reactions: II. Diffusion and Transport Effects," *ibid.*, **27**, p. 247 (1981).

Blackwood, J. D., and F. K. McTaggart, "Reaction of Carbon with Atomic Gases," *Aust. J. Chem.*, **12**, 533 (1959).

deBoor, C., "On Calculating with B-Splines," *J. Approx. Theory*, **6**(1), p. 50 (1972).

deBoor, C., *A Practical Guide to Splines*, Springer-Verlag, New York (1978).

Dutta, S., and C. Y. Wen, "Reactivity of Coal and Char. 2. In Oxygen-Nitrogen Atmosphere," *Ind. Eng. Chem. Process Des. Dev.*, **16**, p. 31 (1977).

Dutta, S., C. Y. Wen, and R. J. Belt, "Reactivity of Coal and Char. 1. In Carbon Dioxide Atmosphere," *ibid.*, **16**, p. 20 (1977).

Gavalas, G. R., "A Random Capillary Model with Application to Char Gasification at Chemically Controlled Rates," *AIChE J.*, **26**, p. 577 (1980).

Gavalas, G. R., "Analysis of Char Combustion Including the Effect of Pore Enlargement," *Comb. Sci. Technol.*, **24**, p. 197 (1981).

Hashimoto, K., and P. L. Silveston, "Gasification: Part I. Isothermal, Kinetic

Control Model for a Solid with a Pore Size Distribution," *AIChE J.*, **19**, p. 259 (1973a).
Hashimoto, K., and P. L. Silveston, "Gasification: Part II. Extension to Diffusion Control," *ibid.*, **19**, p. 268 (1973b).
Hindmarsh, A. C., "Preliminary Documentation of GEARIB: Solution of Implicit Systems of Ordinary Differential Equations with Banded Jacobian," LL Laboratory, UCID-30130 (Feb., 1976).
Howard, J. B., G. C. Williams, and D. H. Fine, "Kinetics of Carbon Monoxide Oxidation in Postflame Gases," 14th Symp. (Int.) on Combustion, p. 975, The Combustion Institute (1973).
Jackson, R., *Transport in Porous Catalysts*, Elsevier, Amsterdam (1977).
Kurylko, L., and R. H. Essenhigh, "Steady and Unsteady Combustion of Carbon," 14th Symp. (Int.) on Combustion, p. 1375, The Combustion Institute (1973).
Laurendeau, N. M., "Heterogeneous Kinetics of Coal Char Gasification and Combustion," *Prog. Energy Comb. Sci.*, **4**, p. 221 (1978).
Madsen, N. K., and R. F. Sincovec, "General Software for Partial Differential Equations," *Numerical Methods for Differential Systems*, L. Lapidus and W. E. Schiesser, Eds., p. 229, Academic Press, New York (1976).
Mon, E., and N. R. Amundson, "Diffusion and Reaction in a Stagnant Boundary Layer about a Carbon Particle. 4: The Dynamical Behavior," *Ind. Eng. Chem. Fund.*, **19**, p. 243 (1980).
Rosner, D. E., and H. D. Allendorf, "Comparative Studies of the Attack of Pyrolytic and Isotopic Graphite by Atomic and Molecular Oxygen at High Temperatures," *A.I.A.A.J.*, **6**, p. 650 (1968).
Ross, I. B., and J. F. Davidson, "The Combustion of Carbon Particles in a Fluidized Bed," *Trans. I. Chem. E.*, **60**, p. 108 (1982).
Simons, G. A., and M. L. Finson, "The Structure of Coal and Char. I. Pore Branching," *Comb. Sci. Technol.*, **19**, p. 217 (1979).
Simons, G. A., "Char Gasification. Part I: Transport Model," *ibid.*, **20**, p. 107 (1979).
Smith, I. W., "The Intrinsic Reactivity of Carbons to Oxygen," *Fuel*, **57**, p. 409 (1978).
Sotirchos, S. V., "Diffusion and Reaction in a Char Particle and in the Surrounding Gas Phase," Ph.D. Dissertation, University of Houston, Houston (1982).
Sotirchos, S. V., and N. R. Amundson, "Diffusion and Reaction in a Char Particle and in the Surrounding Gas Phase. Two Limiting Models," *Ind. Eng. Chem. Fund.* **23**, 180 (1984a).
Sotirchos, S. V., and N. R. Amundson, "Diffusion and Reaction in a Char Particle and in the Surrounding Gas Phase. A Continuous Model," *Ind. Eng. Chem. Fund.* **23**, 191 (1984b).
Sotirchos, S. V., E. Mon, and N. R. Amundson, "Combustion of Coke Deposits in a Catalyst Pellet," *Chem. Eng. Sci.*, **38**, p. 55 (1983).
Srinivas, B., and N. R. Amundson, "Intraparticle Effects in Char Combustion. III. Transient Studies," *Ind. Eng. Chem. Fund.*, **60**, p. 728 *Ind. J., Chem. Eng.*, **59**, 728 (1981).
Sundaresan, S., and N. R. Amundson, "Diffusion and Reaction in a Stagnant Boundary Layer about a Carbon Particle. 7. Transient Behavior and Effect of Water Vapor," *AIChE J.*, **27**, p. 679 (1981).
Ubhayakr, S. K., and F. A. Williams, "Burning and Extinction of a Laser-Ignited Carbon Particle in Quiescent Mixtures of Oxygen and Nitrogen," *J. Electrochem. Soc.*, **123**, p. 747 (1976).
Zamoluev, V. K., L. N. Mukhanova, and E. M. Tait, "The Thermophysical and Mechanical Properties of Highly Carbonized Polymeric Materials," *Proc. Acad. Sci.*, USSR, Chem. Techn. Sect., **133**(5), p. 127 (1960).
Zygourakis, K., L. Arri, and N. R. Amundson, "Studies on the Gasification of a Single Char Particle," *Ind. Eng. Chem. Fund.*, **21**, p. 1 (1982).

Manuscript received January 10, 1983; revision received June 28, 1983 and accepted July 1, 1983.

Part II: Transient Analysis of a Shrinking Particle

The diffusion and reaction model developed in a previous paper is extended allowing for shrinkage of the char particles. It is shown that possible shrinkage, arising from disintegration of the solid structure at a certain conversion level, modifies severely the extinction behavior of the reacting particles. Specifically, the region of ambient temperature and particle radius in which the predictions of the nonisothermal and of the isothermal versions of the model differ significantly becomes smaller. However, the particle shrinkage does not affect the ignition phenomena observed since a particle usually ignites at low conversion levels where the radius change is still negligible.

S. V. SOTIRCHOS and N. R. AMUNDSON

Department of Chemical Engineering
University of Houston
Houston, TX 77004

SCOPE

In Part I, we investigated the transient behavior of char particles in an oxidizing environment. The dynamic model was built on the assumption that the radius of the reacting particles remains constant during the process. This assumption stems from the supposition that the porous solid structure does not collapse at high conversion levels. Several experimental studies, however, indicate that the above may not be true for some types of char. For instance, the char samples used in the experiments of Dutta et al. (1977) disintegrated into smaller fractions at high conversions (above 80%). Also, shrinkage of burning carbon particles in a fluidized-bed combustor is suggested by the experimental data of Ross and Davidson (1982) that show diminishing concentration of CO_2 in the products at intermediate and high conversion levels.

This part of our study focuses on the transient behavior of shrinking particles. As our pseudosteady-state computations (Sotirchos and Amundson, 1984a, b) and the results in Part I have shown, the solution structure of the system depends strongly on the size of the particle and on the intraparticle thermal gradients. Because of the very low thermal conductivity of the ash layer and of the high conversion layers that surround the inner core of a reacting particle, possible particle shrinkage has a direct effect not only on the size of the particle but also on the intraparticle temperature differences. Consequently, significant differences between the behavior of shrinking and nonshrinking particles must be expected.

To allow for changes in the particle size, we assume that shrinkage arises from disintegration of the solid structure at some conversion level which is treated as a model parameter. Our analysis chiefly concentrates on the changes introduced in the extinction behavior of the reacting particles. As the results from the transient model for particles of constant radius (See Part 1) have shown, the particles usually ignite at low average conversion levels, where the conversion at the surface of the particle is well below the disintegration threshold.

Present address of S. V. Sotirchos: Department of Chemical Engineering, University of Rochester, Rochester, NY 14627.